CHAPTER III

EHD INSTABILITY OF A NEMATIC LIQUID CRYSTAL UNDER A TRANSVERSE ELECTRIC FIELD

3.1 Introduction

As we have discussed in Chapter I, nematic liquid crystals with negative or weakly positive dielectric anisotropy and positive conductivity anisotropy exhibit electrohydrodynamic (END) instabilities under the action of an external electric field above a certain threshold value. This phenomenon has been studied extensively with the *standard* geometry in which the electric field is applied across the thickness of a homogeneously aligned nematic liquid crystal (NLC) film. As was described in chapter I, the phenomenon is very well understood as arising from the bend fluctuation of the director field leading to space-charge formation due to conductivity anisotropy. Under the action of an AC electric field, the phenomenon has two distinct frequency regimes. At frequencies lower than the typical charge relaxation rate of the sample, the space-charges can follow the frequency of the electric field and we get the *conduction regime.* The curvature of the director does not change sign with that of the field. On the other hand, at higher frequencies it is the director distortion that oscillates at the frequency of the external electric field, while the space charge

distribution does not change sign. The latter is referred to as the dielectric regime. Dubois-Violette *et al.* (1971) gave a one-dimensional model for the AC instability in which the boundary conditions are ignored. Later Smith *et al.* (1975) extended the theory for squarewave excitation and also approximately included the boundary effects by using appropriately *renormalised* values of the physical parameters. Later Madhusudana *et al.* (1987, 1988) extended AC calculations by taking into account the flexoelectric contributions. They have shown that in a range of very low frequencies, the director field develops additional twist distortions leading to the formation of oblique rolls.

More recently Bodenschatz *et al.* (1988) have developed a three-dirriensional model for AC excitation. In their first calculations they neglected the flexoelectric terms arid have approximately taken into account the boundary conditions by using the Galerkin approximation to solve the problem. Near the threshold, one can choose sinusoidal spatial variations along the X direction. The Z-dependence of the variables should be chosen such that the boundary conditionsat $Z = 0$ and d are satisfied. The gross symmetry of different variables can be guessed by the equations. In the Galerkin approximation, simple trial functions are chosen which satisfy the boundary conditions but these do not satisfy the differential equations exactly. The relevant amplitudes are however chosen so that they satisfy the equations which are appropriately averaged over the thickness of the sample. Later Kramer *et al.* (1989) extended the calculations by taking into account the flexoelectric terms. Their results arc shown in figures 3.1 and **3.2.**

In this chapter we discuss the EHD instabilities in a different geometry. Were the electric field is applied in the plane of a homogeneously aligned NLC film, such that the field is orthogonal to the undistorted director. The observations are made in a

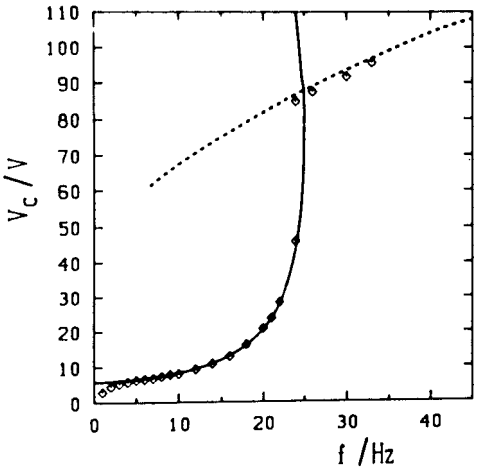

Fig.3.1: Threshold voltage (V_c) as a function of frequency of a vertical field for MBBA parameters (Kramer *et al.*, 1989).

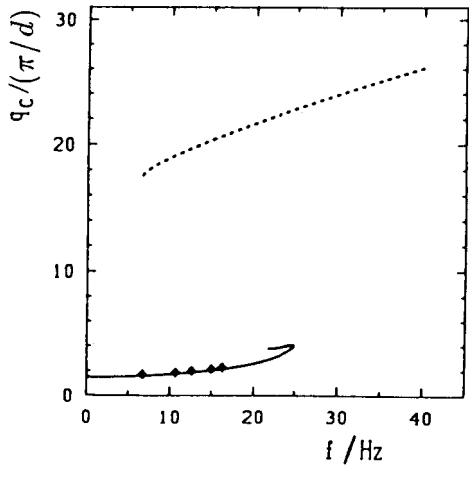

Fig.3.2: Wave number q_c in units π/d as a function of frequency of a vertical field for MBBA parameters (Kramer et al., 1989).

direction normal to the plates as usual. There have been some early experimental studies (Williams, 1972, and Chistyakov and Vistin, 1974) on EHD instabilities in this geometry. However, no theoretical analysis of the problem has hitherto been reported. We present in this chapter a theoretical analysis of this problem for an applied AC field. The results of our theory (Figs.3.3 and 3.5) are broadly similar to the results in the usual geometry (Figs.3.1 and 3.2). Apart from the similarities observed in normal and transverse geometries, there are also some important differences. We have also conducted some experiments in this geometry which will be discussed later in this chapter. The experimental phase diagrams (Figs.3.10 and 3.11) are in broad agreement with the theoretical calculations.

3.2 Theoretical Analysis

We consider a nematic liquid crystal film of thickness d and having an infinite extent in the XY plane. The electric field E_y is applied along the Y axis such tliat it is acting in a transverse direction to the undistorted director $\hat{n}$ which is along the X-axis. Above a critical field, the EHD instabilities develop in the medium resulting in a periodic twist distortion of the director field. Let this distortion be described by an angle ϕ arid further the wavevector associated with such a distortion be along the X axis, with convective rolls being along the Y direction. There is an additional distortion in the director field out of the XY plane due to the flexoelectric contributions and this is described by an angle θ. Therefore the distorted director field is written as $\hat{n} = (\cos\theta\ \cos\phi,\ \cos\theta\ \sin\phi,\ \sin 0)$. Near the onset of EHD instability, since the amplitudes are expected to be small, the EHD equations are linearised following tlie procedure described in Chapter 1. Using the usual riotation, we get the following equations.

a) The Poisson equation

$$\nabla.\vec{D} = 4\pi Q$$

where $\vec{D} = \epsilon_\perp \vec{E} + \Delta\epsilon(\hat{n}\cdot\vec{E})\hat{n} + 4\pi\vec{P}$, and P is the flexoelectric polarisation. This leads to

$$\epsilon_\parallel \frac{\partial E_x}{\partial x} + \epsilon_\perp \frac{\partial E_z}{\partial z} + \Delta\epsilon E_y \frac{\partial \phi}{\partial x} + 4\pi(e_1 + e_3)\frac{\partial^2\theta}{\partial x \partial z} - 4\pi Q = 0 \qquad (3.1)$$

where e_1 and e_3 are the flexoelectric coefficients of the medium, E_x and E_z arise from space charge densities.

b) The charge conservation equation $\frac{\partial Q}{at} + \mathrm{V}\,.\,J = 0$ gives rise to

$$\frac{\partial Q}{\partial t} + \sigma_\parallel \frac{\partial E_x}{\partial x} + \sigma_\perp \frac{\partial E_z}{\partial z} + \Delta\sigma E_y \frac{\partial \phi}{\partial x} = 0 \qquad (3.2)$$

c) The torque balance equation along Y and Z axes are given by

$$\gamma_1 \frac{\partial \phi}{\partial t} + \alpha_2 \frac{\partial v_y}{\partial x} - K_3 \frac{\partial^2 \phi}{\partial x^2} - K_2 \frac{\partial^2 \phi}{\partial z^2} - \frac{\Delta\epsilon}{4\pi}[E_x + E_y \phi]E_y$$

$$- (e_1 - e_3)E_y \frac{\partial \theta}{\partial z} = 0 \qquad (3.3)$$

$$\gamma_1 \frac{\partial \theta}{\partial t} + \alpha_3 \frac{\partial v_x}{\partial z} + \alpha_2 \frac{\partial v_z}{\partial x} - K_3 \frac{\partial^2 \theta}{\partial x^2} - K_1 \frac{\partial^2 \theta}{\partial z^2}$$

$$+ (e_1 - e_3)E_y \frac{\partial \phi}{\partial z} + e_1 \frac{\partial E_x}{\partial z} + e_3 \frac{\partial E_z}{\partial x} = 0 \qquad (3.4)$$

d) The x component of equation of motion is

$$\frac{\partial P}{\partial x} - (\alpha_1 + \alpha_4 + \alpha_5 + \alpha_6)\frac{\partial^2 v_x}{\partial x^2} - \frac{1}{2}(\alpha_4 + \alpha_6 - \alpha_3)\frac{\partial^2 v_z}{\partial x \partial z}$$

$$- \frac{1}{2}(\alpha_4 + \alpha_6 + \alpha_3)\frac{\partial^2 v_x}{\partial z^2} - \alpha_3 \frac{d^2\theta}{dz\,dt} = 0 \qquad (3.5)$$

e) The Y component of equation of motion is given by

$$\frac{1}{2}(\alpha_4 + \alpha_5 - \alpha_2)\frac{d^2 v_y}{\partial x^2} + \frac{1}{2}\alpha_4 \frac{d^2 v_y}{\partial z^2} + \alpha_2 \frac{\partial^2 \phi}{\partial x \partial t} + E_y Q = 0 \tag{3.6}$$

f) The Z-component of equation of motion becomes

$$\frac{\partial P}{\partial z} - \frac{1}{2}(\alpha_4 + \alpha_5 + \alpha_2)\frac{\partial^2 v_x}{\partial x \partial z} - \frac{1}{2}(\alpha_4 + \alpha_5 - \alpha_2)\frac{\partial^2 v_z}{\partial x^2}$$

$$- \alpha_4 \frac{d^2 v_z}{\partial z^2} - \alpha_2 \frac{d^2 \mathbf{0}}{\partial x \partial t} = 0 \tag{3.7}$$

where P is the pressure. In the above three equations of motion, the inertial terms are negligible at the frequencies of interest and hence are neglected (Dubois-Violette *et al.*, 1971).

g) Assuming the NLC medium to be incompressible we can write $\nabla \cdot \vec{v} = 0$ and hence

$$\frac{\partial v_x}{\partial x} + \frac{\partial v_z}{\partial z} = 0 \tag{3.8}$$

h) From the Maxwell relation, $\nabla \times E = 0$, we get,

$$\frac{\partial E_x}{\partial z} - \frac{\partial E_z}{\partial x} = 0 \tag{3.9}$$

Eliminating pressure term P from equations **(3.5)** and **(3.7)** we get,

$$\alpha_2 \frac{\partial^3 \theta}{\partial x^2 \partial t} - \alpha_3 \frac{\partial^3 \theta}{\partial z^2 \partial t} - \left[\alpha_1 + \alpha_6 + \left(\frac{\alpha_4 + \alpha_5 - \alpha_2}{2}\right)\right] \frac{\partial^3 v_x}{\partial x^2 \partial z}$$

$$+ \left(\frac{\alpha_4 - \alpha_6 + \alpha_3}{2}\right) \frac{\partial^3 v_z}{\partial x \partial z^2} - \left(\frac{\alpha_4 + \alpha_6 + \alpha_3}{2}\right) \frac{\partial^3 v_x}{\partial z^3}$$

$$+ \left(\frac{\alpha_4 + \alpha_5 - \alpha_2}{2}\right) \frac{\partial^3 v_z}{\partial x^3} = 0 \tag{3.10}$$

The boundary conditions to be considered in solving these equations are, at $Z = 0$ and d (at the two surfaces of NLC film)

$$(\theta, \phi, Q, E_x, E_z, v_x, v_y, v_z) = 0$$

The X-dependence of these quantities in the above equations can be satisfied by sinusoidal functions of the type sin qx. Following the earlier work of Bodenschatz *et* al. *(1988)* and Kramer *et* al. *(1989)* the Z-dependences are taken into account in a Galerkin approximation by chosing trial function solutions. By inspection of the above equations *(3.1-3.10)* the following solutions are assumed for the variables:

$$\begin{aligned}
\phi &= \phi(t) \sin qx \ \sin pz; \quad Q = Q(t) \ \cos qx \ \sin pz; \\
E_x &= E_x(t) \sin qx \ \sin pz; \quad v, = v_x(t) \sin qx \ \sin pz; \\
v, &= v_y(t) \ \cos qx \ \sin pz; \quad \theta = \theta(t) \sin qx \ \sin 2pz; \\
E_z &= E_z(t) \ \cos qx \ \sin 2pz; \quad v, = v_z(t) \ \cos qx \ \sin 2pz
\end{aligned} \tag{3.11}$$

where p $= \pi/d$.

We now use the Galerkine approximation, i.e., we integrate equations *(3.1-3.10)* after substituting the above functional forms for the solutions and we average over the cell thickness d in order to get the following equations

$$\epsilon_{\|} q E_x + 2\epsilon_{\perp} p I_1 E_z + \Delta\epsilon E_y q\phi + 8\pi(e_1 + e_3) pq I_1 \theta - 4\pi Q = 0 \tag{3.12}$$

where

$$I_1 = \frac{\int_o^d \sin pz \ \cos \ 2pz \, dz}{\int_o^d \sin^2 pz \ dz} \tag{3.13}$$

Equation *(3.2)* gives rise to

$$\frac{\partial Q}{\partial t} + \sigma_{\|} q E_x + 2\sigma_{\perp} p I_1 E_z + \Delta\sigma E_y q\phi = 0 \ . \tag{3.14}$$

Equation (3.3) is modified into

$$\gamma_1 \frac{\partial \phi}{\partial t} - \alpha_2 q v_y + K_3 q^2 \phi + K_2 p^2 \phi - \frac{\Delta \epsilon}{4\pi}(E_y^2 \phi + E_y E_x) - 2(e_1 - e_3) E_y p I_1 \theta = 0 \ . \tag{3.15}$$

Equation (3.4) leads to

$$\gamma_1 \frac{\partial \theta}{at} + \alpha_3 p I_2 v_x - \alpha_2 q v_z + (k_3 q^2 + 4 k_1 p^2)\theta + (\mathrm{el} - e_3) E_y p I_2 \phi + e_1 p I_2 E_x - e_3 q E_z = 0 \ . \tag{3.16}$$

where

$$I_2 = \frac{\int_o^d \sin 2pz \cos pz \, \mathrm{dr}}{\int_o^d \sin^2 2pz \, dz} \tag{3.17}$$

Equation (3.10) reduces to

$$-\alpha_2 q^2 \frac{\partial \theta}{\partial t} + 4\alpha_3 p^2 \frac{\partial \theta}{\partial t} + \left\{ \alpha_1 + \alpha_6 + \frac{\alpha_4 + \alpha_5 - \alpha_2}{2} \right\} p q^2 I_2 v_x + 2(\alpha_4 - \alpha_6 + \alpha_3) p^2 q v_z - \frac{1}{2}(\alpha_4 + \alpha_6 + \alpha_3) p^3 I_2 v_x + \left(\frac{\alpha_4 + \alpha_5 - \alpha_2}{2} \right) q^3 v_z = 0 \ . \tag{3.18}$$

Equation (3.6) becomes

$$-\frac{1}{2}\alpha_4 p^2 v_y - \left(\frac{\alpha_4 + \alpha_5 - \alpha_2}{2} \right) q^2 v_y + \alpha_2 q \frac{\partial \phi}{\partial t} + E_y Q = 0 \tag{3.19}$$

Equation (3.8) is modified as

$$q v_x + 2 p I_1 v_z = 0 \tag{3.20}$$

Equation (3.9) reduces to

$$q E_z \mathbf{t} \, p I_2 E_x = 0 \ . \tag{3.21}$$

From equation *(3.19)*

$$v_y = \frac{2(E_y Q + \alpha_2 q \frac{\partial \phi}{} .\partial t)}{\alpha_4 p^2 + \eta q^2} \tag{3.22}$$

where $\eta = \alpha_4 + \alpha_5 - \alpha_2$.

From equation *(3.20)*

$$v, = -2SI_1 v_z \tag{3.23}$$

where $S = p/q$.

From equation *(3.21)*

$$E_z = -SI_2 E_x \ . \tag{3.24}$$

Substituting for $v_y, v,$ and $E_{,,}$ equation *(3.12)* becomes,

$$\epsilon_{||} q E_x - 2\epsilon_\perp p S I_1 I_2 E_x + \Delta\epsilon E_y q \phi + 8\pi(e_1 + e_3) pq I_1 \theta - 4\pi Q = 0$$

$$E_x = \frac{4\pi Q - \Delta\epsilon E_y q\phi - 8\pi(e_1 + e_3) pq I_1 \theta}{(\epsilon_{||} - 2\epsilon_\perp S^2 I_1 I_2) q} \tag{3.25}$$

From equation *(3.18)* we get,

$$v_z = \left(\frac{\alpha_2 - 4\alpha_3 S^2}{\beta q} \right) \frac{\partial \theta}{\partial t} \tag{3.26}$$

where

$\beta = (\alpha_4 + \alpha_6 + \alpha_3) S^4 I_1 I_2 + 2(\alpha_4 - \alpha_6 + \alpha_3) S^2 - 2(\alpha_1 + \alpha_6 + \frac{\eta}{2}) S^2 I_1 I_2 + \frac{1}{2}\eta.$

Using equations *(3.22)* to (3.26), we can eliminate other variables in favour of $Q, 4$ and θ and rewrite equations *(3.14)* to *(3.16)* as

$$\frac{\partial Q}{\partial t} + \frac{4\pi(\sigma_{||} - 2\sigma_\perp S^2 I_1 I_2) Q}{\epsilon_{||} - 2\epsilon_\perp S^2 I_1 I_2}$$

$$+ (\sigma_{||} - 2\sigma_\perp S^2 I_1 I_2) \left\{ \frac{\Delta\sigma}{\sigma_{||} - 2\sigma_\perp S^2 I_1 I_2} - \frac{\Delta\epsilon}{\epsilon_{||} - 2\epsilon_\perp S^2 I_1 I_2} \right\} E_y q \phi$$

$$- \frac{8\pi(e_1 + e_3)(\sigma_{||} - 2\sigma_\perp S^2 I_1 I_2)}{(\epsilon_{||} - 2\epsilon_\perp S^2 I_1 I_2)} pq I_1 \theta = 0 \ , \tag{3.27}$$

$$\left\{\gamma_1 - \frac{2\alpha_2^2}{\eta + \alpha_4 S^2}\right\}\frac{\partial \phi}{\partial t} + \left\{K_3 q^2 + K_2 p^2 - \frac{\Delta\epsilon}{4\pi}E_y^2\left(1 - \frac{\Delta\epsilon}{\epsilon_{\|} - 2\epsilon_{\perp}S^2 I_1 I_2}\right)\right\}\phi$$

$$- \left\{\frac{2\alpha_2}{\eta + \alpha_4 S^2} + \frac{\Delta\epsilon}{\epsilon_{\|} - 2\epsilon_{\perp}S^2 I_1 I_2}\right\}\frac{E_y}{q}Q$$

$$+ 2\left\{\frac{\Delta\epsilon(e_1 + e_3)}{\epsilon_{\|} - 2\epsilon_{\perp}S^2 I_1 I_2} - (e_1 - e_3)\right\}E_y p I_1 \theta = 0 \qquad (3.28)$$

and

$$\left\{\gamma_1 - \frac{(\alpha_2 - 4\alpha_3 S^2)(\alpha_2 + 2\alpha_3 S^2 I_1 I_2)}{\beta}\right\}\frac{\partial \theta}{\partial t}$$

$$+ \left\{K_3 + 4K_1 S^2 - \frac{8\pi(e_1 + e_3)^2 S^2 I_1 I_2}{\epsilon_{\|} - 2\epsilon_{\perp}S^2 I_1 I_2}\right\}q^2\theta$$

$$+ \left\{(e_1 - e_3) - \frac{\Delta\epsilon(e_1 + e_3)}{\epsilon_{\|} - 2\epsilon_{\perp}S^2 I_1 I_2}\right\}E_y p I_2 \phi$$

$$+ \frac{4\pi(e_1 + e_3)S I_2}{\epsilon_{\|} - 2\epsilon_{\perp}S^2 I_1 I_2}Q = 0 \qquad (3.29)$$

Equations (3.27-3.29) are simplified to read as follows:

$$\frac{\partial Q}{\partial t} + \frac{1}{\tau}Q + \sigma_H E_y q\phi - A6 = 0 \qquad (3.30)$$

$$\frac{\partial \phi}{\partial t} + \frac{1}{T_\phi}\phi - BE_y Q + 2I_1 C_1 E_y \theta = 0 \qquad (3.31)$$

$$\frac{\partial \theta}{\partial t} + \frac{1}{T_\theta}\theta - I_2 C_2 E_y \phi + DQ = 0 \qquad (3.32)$$

where

$$\sigma_H = \sigma_c\left(\frac{\Delta\sigma}{\sigma_c} - \frac{\Delta\epsilon}{\epsilon_c}\right);\ \epsilon_c = \epsilon_{\|} - 2\epsilon_{\perp}S^2I_1I_2;\ \sigma_c = \sigma_{\|} - 2\sigma_{\perp}S^2I_1I_2;$$

$$\frac{1}{\tau} = \frac{4\pi\sigma_c}{\epsilon_c};\ \frac{1}{T_\phi} = \frac{1}{\eta_1}\left\{K_3 + 4K_2S^2 - \frac{\Delta\epsilon E_y^2\epsilon_{\perp}(1 - 2S^2I_1I_2)}{4\pi q^2\epsilon_c}\right\}q^2;$$

$$\frac{1}{T_\theta} = \frac{1}{\eta_2}\left\{K_3 + K_1S^2 - \frac{8\pi(e_1 + e_3)^2I_1I_2S^2}{\epsilon_c}\right\}q^2;$$

$$A = \frac{8\pi\sigma_c(e_1 + e_3)pqI_1}{\epsilon_c};\ B = \frac{1}{\eta_1}\left[\frac{2\alpha_2}{\alpha_4S^2 + \eta} + \frac{\Delta\epsilon}{\epsilon_c}\right]\frac{1}{q};$$

$$C_1 = \frac{p}{\eta_1}\left\{\frac{\Delta\epsilon(e_1 + e_3)}{\epsilon_c} - (e_1 - e_3)\right\};\quad C_2 = C_1\frac{\eta_1}{\eta_2}$$

$$D = \frac{4\pi(e_1 + e_3)SI_2}{\epsilon_c\eta_2};\ \eta_1 = \left(\gamma_1 - \frac{2\alpha_2^2}{\alpha_4S^2 + \eta}\right);$$

$$\eta = (\alpha_4 + \alpha_5 - \alpha_2);\ \eta_2 = \left\{\gamma_1 - \frac{(\alpha_2 - 4\alpha_3S^2)(\alpha_2 + 2\alpha_3S^2I_1I_2)}{\beta}\right\};$$

$$S = p/q;\ I_1 = -\frac{4}{3\pi};\ I_2 = \frac{8}{3\pi}$$

These equations (3.30 - 3.32) form a set of ordinary differential equations in Q, ϕ and 0. In order to simplify the problem we solved the above set of equations for the case of square wave excitation (Smith et al., 1975). Assuming solutions of the form $Q = Q'e^{\lambda t}$, $\phi = \phi'e^{\prime\lambda t}$ and $\theta = \theta'e^{\lambda t}$, the existence of non-trivial solutions require that the determinant of the coefficients of the amplitudes Q', ϕ' and θ' should vanish,

$$\begin{vmatrix} (\lambda + \frac{1}{\tau}) & \sigma_H E_y q & -A \\ -BE_y & (\lambda + \frac{1}{T_\phi}) & 2I_1C_1E_y \\ D & -I_2C_2E_y & (\mathrm{A} + \frac{1}{T_\theta}) \end{vmatrix} = 0 \qquad (3.33)$$

Expanding this determinant we get,

$$\lambda^3 + \lambda^2\left[\frac{1}{T_\theta}+\frac{1}{T_\phi}+\frac{1}{\tau}\right]$$

$$+ \lambda\left[\frac{1}{\tau}\left(\frac{1}{T_\theta}+\frac{1}{T_\phi}\right)+\frac{1}{T_\theta T_\phi}+2I_1I_2C_1C_2E_y^2+B\sigma_H E_y^2 q+AD\right]$$

$$+ \frac{1}{\tau}\left[\frac{1}{T_\theta T_\phi}+2I_1I_2C_1C_2E_y^2\right]+\frac{B\sigma_H E_y^2 q}{T_\theta}-ABC_2I_2E_y^2$$

$$+ 2\sigma_H C_1 D I_1 q E_y^2+\frac{AD}{T_\phi}=0\ . \tag{3.34}$$

In the conduction regime we can write,

$$\begin{aligned} Q(t=0) &= -Q(t=T/2) \\ \theta(t=0) &= -\theta(t=T/2) \\ \phi(t=0) &= \phi(t=T/2)\ . \end{aligned} \tag{3.35}$$

The general form of Q is written as,

$$Q=\sum_{i=1}^{3} Q_i e^{\lambda_i t}\ . \tag{3.36}$$

Then using equation **(3.35)** we can write

$$\sum_{i=1}^{3} Q_i(1+e^{\lambda_i T/2})=0\ . \tag{3.37}$$

Similarly we can write

$$\sum_{i=1}^{3} \theta_i(1+e^{\lambda_i T/2})=0 \tag{3.38}$$

and

$$\sum_{i=1}^{3} \phi_i(1-e^{\lambda_i T/2})=0 \tag{3.39}$$

Equation *(3.31)* becomes,

$$\left(\lambda_i + \frac{1}{T_\phi}\right)\phi_i - BE_y Q_i + 2I_1 C_1 E_y \theta_i = 0 \tag{3.40}$$

and equation *(3.32)* becomes,

$$\left(\lambda_i + \frac{1}{T_\theta}\right)\theta_i - I_2 C_2 E_y \phi_i + DQ_i = 0\ . \tag{3.41}$$

Eliminating Q_i from the equations *(3.40)* and *(3.41)* we get,

$$\theta_i = t_i \phi_i \tag{3.42}$$

where $$t_i = \frac{I_2 B C_2 E_y^2 - D(\lambda_i + \frac{1}{T_\phi})}{BE_y(\lambda_i + \frac{1}{T_\theta}) + 2I_1 C_1 D E_y}\ .$$

Further equation *(3.30)* becomes,

$$\left(\lambda_i + \frac{1}{\tau}\right) Q_i + (\sigma_H E_y q - A t_i)\phi_i = 0 \tag{3.43}$$

or

$$Q_i = g_i \phi_i \tag{3.44}$$

where $$g_i = \frac{A t_i - \sigma_H E_y q}{\lambda_i + \frac{1}{\tau}}$$

Using equations *(3.42)* and *(3.44)* in equations *(3.37)* and *(3.38)* we get

$$\begin{aligned} \sum \phi_i g_i (1 + e^{\lambda_i T/2}) &= 0 \\ \sum \phi_i t_i (1 + e^{\lambda_i T/2}) &= 0 \quad \text{and} \\ \sum \phi_i (1 - e^{\lambda_i T/2}) &= 0 \end{aligned} \tag{3.45}$$

The determinant of the coefficients of ϕ_1, ϕ_2 and ϕ_3 in the above equations should also vanish

$$\begin{vmatrix} g_1(1 + e^{\lambda_1 T/2}) & g_2(1 + e^{\lambda_2 T/2}) & g_3(1 + e^{\lambda_3 T/2}) \\ t_1(1 + e^{\lambda_1 T/2}) & t_2(1 + e^{\lambda_2 T/2}) & t_3(1 + e^{\lambda_3 T/2}) \\ (1 - e^{\lambda_1 T/2}) & (1 - e^{\lambda_2 T/2}) & (1 - e^{\lambda_3 T/2}) \end{vmatrix} = 0 \tag{3.46}$$

For a given set of values of the material parameters (Table *2.1)* and for a given value of the applied field E_y, equation *(3.34)* is first solved to obtain λ_i. These values of λ_i are then substituted in equation *(3.46)*. The value E, for which equation *(3.46)* is satisfied, gives the threshold field, E_{th} of the instability in the conduction regime. In the dielectric regime, the boundary conditions are,

$$\begin{aligned} Q(t=0) &= Q(t=T/2) \\ \theta(t=0) &= \theta(t=T/2) \\ \phi(t=0) &= -\phi(t=T/2) \end{aligned} \tag{3.47}$$

Using these boundary conditions the equations *(3.37)* to *(3.39)* becomes,

$$\begin{aligned} \sum g_i\phi_i(1-e^{\lambda_i T/2}) &= 0 \\ \sum t_i\phi_i(1-e^{\lambda_i T/2}) &= 0 \quad \text{and} \\ \sum \phi_i(1+e^{\lambda_i T/2}) &= 0\ . \end{aligned} \tag{3.48}$$

Then the determinant of the coefficients of ϕ_1, ϕ_2 and ϕ_3 is written as

$$\begin{bmatrix} g_1(1-e^{\lambda_1 T/2}) & g_2(1-e^{\lambda_2 T/2}) & g_3(1-e^{\lambda_3 T/2}) \\ t_1(1-e^{\lambda_1 T/2}) & t_2(1-e^{\lambda_2 T/2}) & t_3(1-e^{\lambda_3 T/2}) \\ (1+e^{\lambda_1 T/2}) & (1+e^{\lambda_2 T/2}) & (1+e^{\lambda_3 T/2}) \end{bmatrix} = 0\ . \tag{3.49}$$

The threshold of dielectric regime is determined using the same procedure as above. Another possible set of solutions of equations *(3.1)* to *(3.10)* are obtained by replacing sin pz by sin $2pz$ and vice versa in *(3.11)*

$$\begin{aligned} \phi &= \phi(t)\sin qx\ \sin 2pz\ ;\quad Q = Q(t)\cos qx\ \sin 2pz\ ; \\ E_x &= E_x(t)\sin qx\ \sin 2pz\ ;\quad v_x = v_x(t)\sin qx\ \sin 2pz\ ; \\ v_y &= v_y(t)\cos qx\ \sin 2pz\ ;\quad \theta = \theta(t)\sin qx\ \sin pz\ ; \\ E_z &= E_z(t)\cos qx\ \sin pz;\quad v_z = v_z(t)\cos qx\ \sin pz \end{aligned} \tag{3.50}$$

Then proceeding as before using the equations *(3.1)* to *(3.10)* and eliminating v_x, E_z and V, we get the following equations :

$$\frac{\partial Q}{\partial t} + \frac{1}{\tau}Q + \sigma_H E_y q\phi - A'\theta = 0 \tag{3.51}$$

$$\frac{\partial \phi}{\partial t} + \frac{1}{T'_\phi}\phi - B'E_y Q + C'_1 I_2 E_y \theta = 0 \tag{3.52}$$

$$\frac{\partial \theta}{\partial t} + \frac{1}{T'_\theta}\theta - 2I_1 C'_2 E_y \phi + D'Q = 0 \tag{3.53}$$

where

$$A' = \frac{4\pi\sigma_c}{\epsilon_c}(e_1+e_3)pqI_2\,;\ \eta'_1 = \gamma_1 - \frac{2\alpha_2^2}{\eta+4\alpha_4 S^2}\,;\ B' = \left(\frac{2\alpha_2}{\eta+4\alpha_4 S^2}+\frac{\Delta\epsilon}{\epsilon_c}\right)\frac{1}{q\eta'_1}\,;$$

$$C'_1 = \frac{p}{\eta'_1}\left\{\frac{\Delta\epsilon(e_1+e_3)}{\epsilon_c} - (e_1-e_3)\right\}\,;\ \eta'_2 = \gamma_1 - \frac{(\alpha_2-\alpha_3 S^2)(\alpha_2+2\alpha_3 S^2 I_1 I_2)}{\beta'}$$

$$\beta' = 4(\alpha_4+\alpha_6+\alpha_3)S^4 I_1 I_2 + \frac{(\alpha_4-\alpha_6+\alpha_3)S^2}{2} - 2\left(\alpha_1+\alpha_6+\frac{\eta}{2}\right)S^2 I_1 I_2 + \frac{\eta}{2}$$

$$C'_2 = \frac{C'_1}{\eta'_2}\eta'_1\,;\quad D' = \frac{8\pi(e_1+e_3)SI_1}{\epsilon_c\eta'_2}$$

$$\frac{1}{T'_\theta} = \frac{q^2}{\eta'_2}\left\{K_3 + K_1 S^2 - \frac{8\pi(e_1+e_3)^2 S^2 I_1 I_2}{\epsilon_c}\right\}$$

$$\frac{1}{T'_\phi} = \left\{K_3 + 4K_2 S^2 - \frac{\Delta\epsilon}{4\pi}\frac{E_o^2}{q^2}\frac{\epsilon_\perp(1-2S^2 I_1 I_2)}{\epsilon_c}\right\}\frac{q^2}{\eta'_1}$$

and all other parameters are as defined after the equation *(3.32)*. Equations *(3.51)* to *(3.53)* are solved as in the previous case.

Figure 3.3 shows the critical voltage (V_{th}) for the onset of the instability calculated for MBBA parameters (Table 3.1) as a function of the reduced frequency $\frac{f}{f_c}\left(f_c = \frac{2\sigma_{\|}}{\epsilon_{\|}}\right)$. The solid lines correspond to the solution Set 1 and the dashed lines to Set 2.

In the dielectric regime the voltage corresponding to the threshold for Set 2 is only marginally greater than that for Set 1. In the conduction regime θ is negligible due to its flexoelectric origin, except at the lowest frequencies of the applied field. The solution Set 2 consists of larger ϕ distortion and larger viscous dissipation which leads to a larger threshold voltage. On the other hand in the dielectric regime, a larger ϕ distortion can lead to a larger relaxation frequency $1/T_\phi$. The threshold of the dielectric regime is determined by the condition that the frequency of the applied field $\simeq 1/T_\phi$. This may be the reason for the thresholds for solution Sets 1 and 2 to have nearly equal values in this regime.

The variation of the critical wavevector (q/p) as a function of the reduced frequency (f/f_c) is shown in figure **3.4.** From these figures it is clear that the general features of transverse instability are similar to those in the case with E along the Z-axis. However, we must note that in the case of the vertical field, the flexoelectric effect destroys the symmetry of the variables about the midplane of tlie sample.

3.3 Experimental Studies

The cell is made of ordinary glass plates which are coated with polyimide and unidirectionally rubbed to get homogeneous alignment of the director. Stainless steel wires of 50 μm diameter are used to apply the transverse electric field. They also serve as spacers (Fig.3.5). The lateral separation between these wires is about **400** μm. The thickness of the cell is measured by using the technique of chan-

Table 3.1

Material parameters of MBBA used in the calculations

$K_1 = 6.1 \times 10^{-7}$ dyne (1)	$\alpha_1 = 6.5$ cP (3)
$K_2 = 4.0 \times 10^{-7}$ dyne (2)	$\alpha_2 = -77$ cP (3)
$K_3 = 7.3 \times 10^{-7}$ dyne (1)	$\alpha_3 = -1.2$ cP (3)
$\epsilon_{\|} = 4.75$ (1)	$\alpha_4 = 83$ cP (3)
$\epsilon_{\perp} = 5.25$ (1)	$\alpha_5 = 46$ cP (3)
$\sigma_{\|} = 0.1 \times 10^{-10} \text{ohm}^{-1}\text{cm}^{-1}$	$\alpha_6 = -34$ cP
$\frac{\sigma_{\|}}{\sigma_{\perp}} = 1.5$ (1)	$(e_1 + e_3) = -7 \times 10^{-4}$ e.s.u. (4)
$\frac{A0}{\sigma_{\perp}} = 0.5$ (1)	$(e_1 - e_3) = 1 \times 10^{-4}$ e.s.u. (5)

1. Penz and Ford, 1972
2. Blinov, 1983
3. de Gennes, 1975
4. Madhusudana and Durand, 1985
5. Dozov et al., 1982.

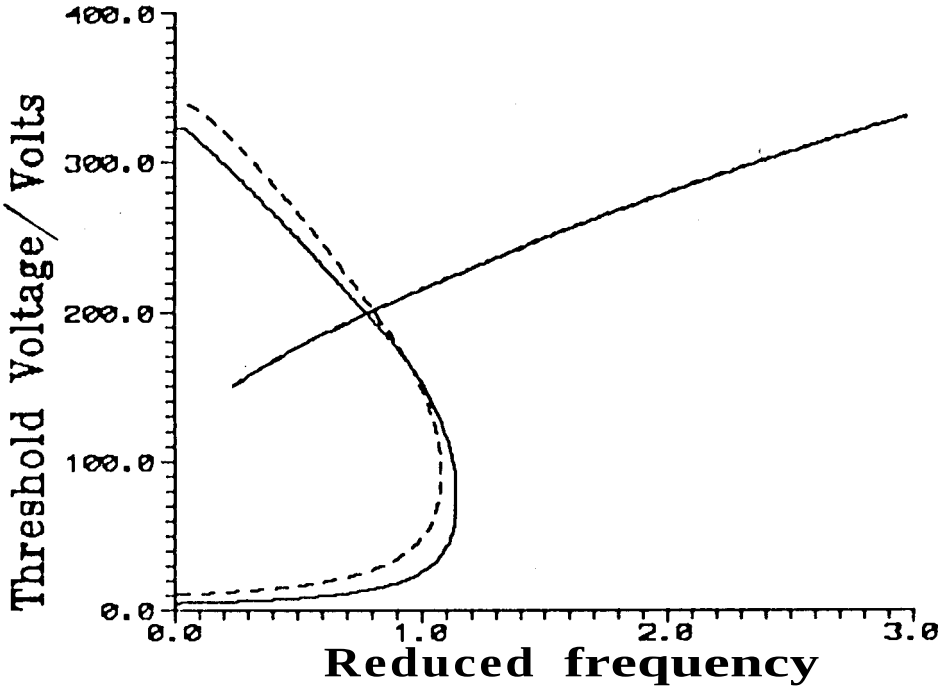

Fig.3.3: Variation of the threshold voltage with reduced frequency obtained from the calculations using MBBA parameters. d=50 μm. Lateral separation between the electrodes is 60 μm. The cut off frequency $f_c = 2\sigma_{\|}/\epsilon_{\|}$.

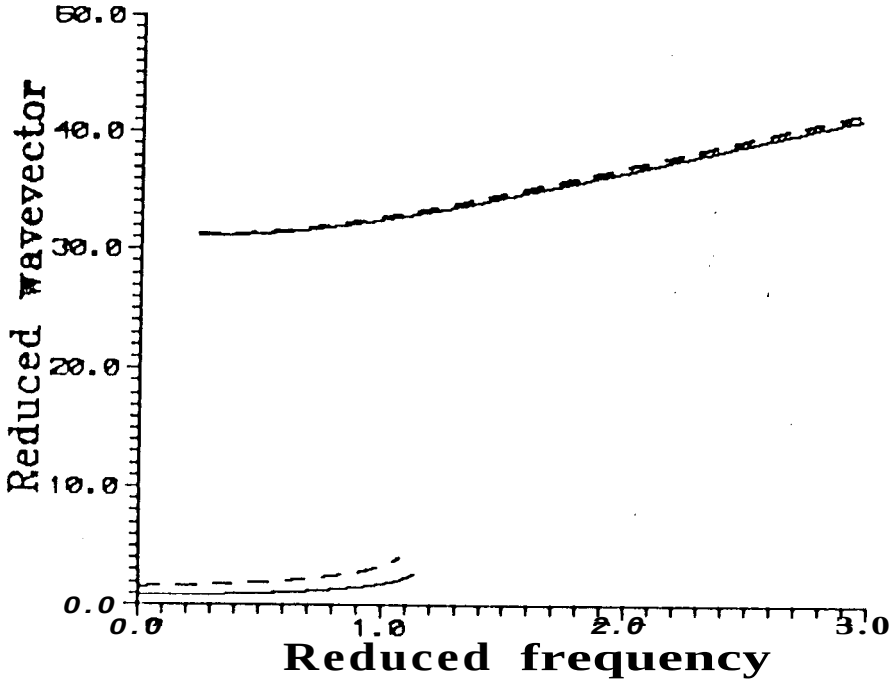

Fig.3.4: Variation of the reduced wavevector (q/p) with reduced frequency (f/f_c) obtained from the calculations using MBBA parameters for the cell particulars used in **Fig.3.3.** Here $q = 2\pi/\lambda$, λ being the wavelength of domains and $\mathbf{p} = \pi/d$.

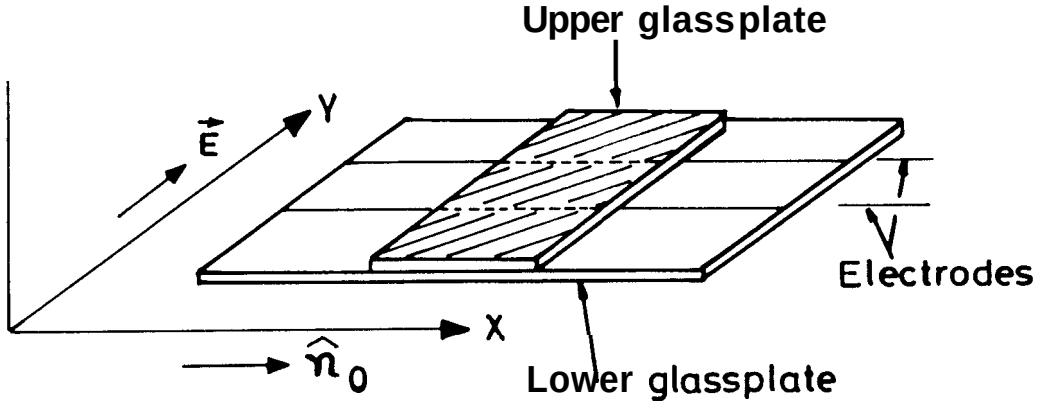

Fig.3.5: The geometry of the cell used in the experiment.

nel spectrum (as described in Chapter II). The material used in the experiments is a room temperature nematic mixture containing 49% (2-methylphenyl)-bis-4-n-butylbenzoate (RO-CE-1700) and 51% 1-n-propyl-4[4-n-ethoxyphenyl]cyclohexane (PCH-302), both of which were obtained from Hoffmann-La Roche Company. The structural formulae of the compounds are shown in figure 3.6.

The cell is placed on the stage of a Leitz polarizing microscope (Orthoplan). A Mettler hot stage (FP82) is used to regulate the temperature of the sample. A Hewlett Packard two channel synthesiser (Model No.3326A) is used to apply the AC field. The EHD instability pattern is observed on a video monitor (Sony-TRINITRON) using a CCD video camera (Sony). The voltage at which the EHD pattern first appears gives the threshold voltage (V_{th}). A block diagram of the experimental set up is shown in figure 3.7. Some photographs of the EHD pattern under transverse field at different frequencies are shown in figure 3.8. Note the decrease of wavelength of the domains as the frequency of the applied field is increased. The photographs taken at voltage much above V_{th} are shown in figure 3.9. As has been noted by earlier workers (Chistyakov and Vistin, 1974) in this geometry, dark bands corresponding to neighbouring roles start from opposite electrodes even with an applied AC field. Our present model does not explain this phenomenon.

At the onset of the instability the director field develops twist distortion. But this cannot be detected in view of the Mauguin criterion (1911). However, at slightly higher voltages, observations clearly indicate that the twist distortion is quite predominant, with the neighbouring convective cells having twist of opposite sense (see the video prints in Fig. 3.10). The high frequency dielectric regime could not be observed as an irregular flow developed in the cell at the very high voltages required at these frequencies.

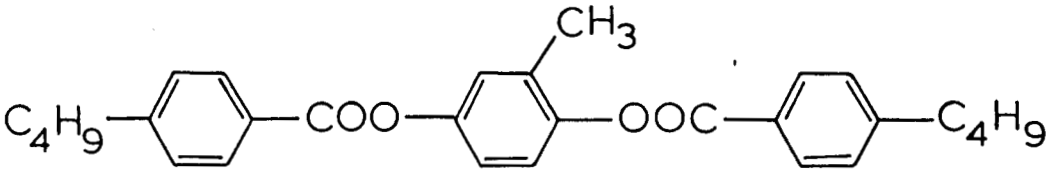

2 – Methylphenyl – bis-4 – n – butylbenzoate

[RO – CE 1700]

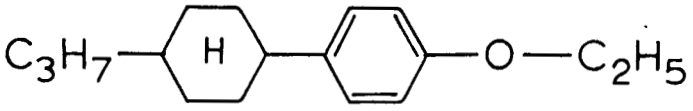

1 – n – propyl – 4(4 – n – ethoxyphenyl)cyclohexane

[PCH – 302]

Fig.3.6: Structural formuale of the compounds used in the nematic mixture.

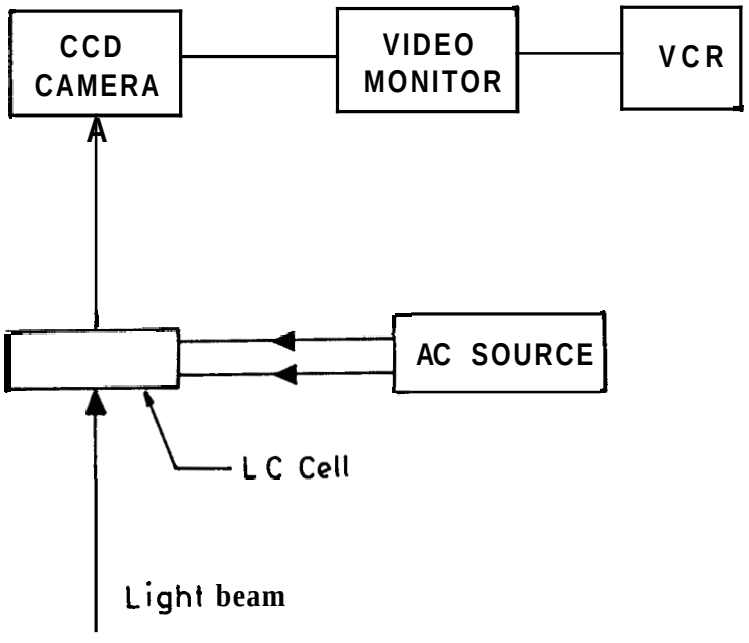

Fig.3.7: Block diagram of the experimental set-up used to record the transverse EHD pattern.

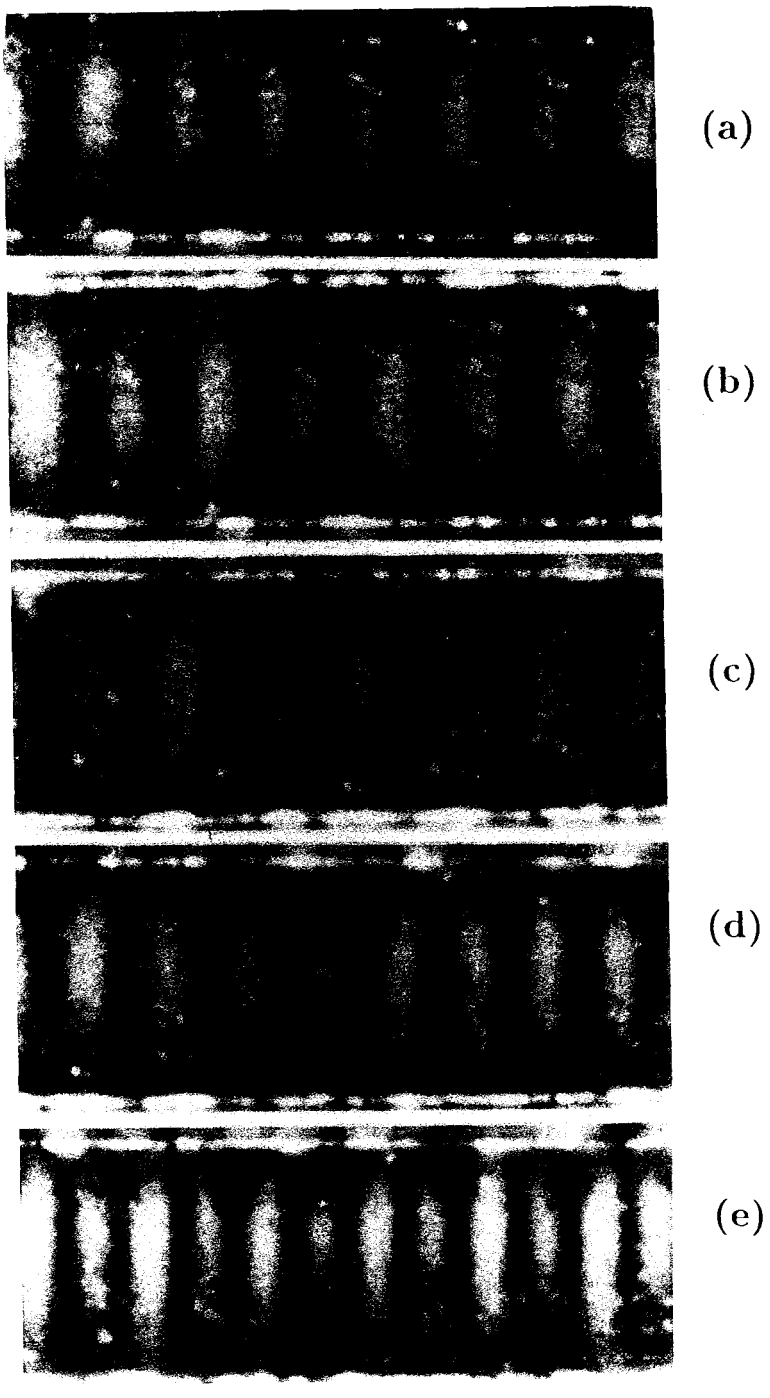

Fig.3.8: Transverse EHD pattern observed at different frequencies. (a) *77* Hz *(24.5* V), (b) *177* Hz *(22.7* V), (c) *577* Hz *(24.1 V)*, (d) *1177* Hz (35.4 V), and (e) *1577* Hz *(48.9 V)*. The cell has a thickness d=12.1 μm and interelectrode space 54.2 μm. The position of the electrodes is on top and bottom sides of each strip with the nematic director parallel to the electrodes. These observations are made with crossed polarisers.

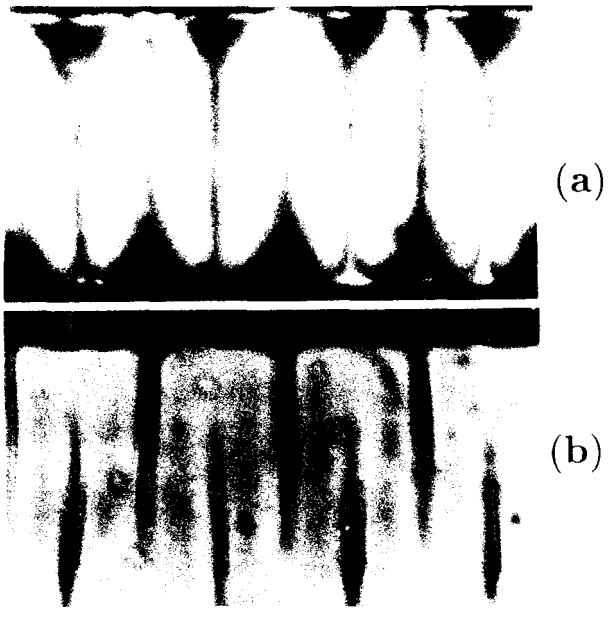

Fig.3.9: Transverse EHD pattern observed in the same cell shown in Fig.3.8 at frequency = 111 Hz. The voltage is 45.5 V which is well above the threshold voltage of 34 V. The photograph **(a)** is taken with tlie polariscr parallel to the director and the analyses crossed with respect to it. The photograph (b) is taken with both the polarises and the analyser parallel to the nematic director.

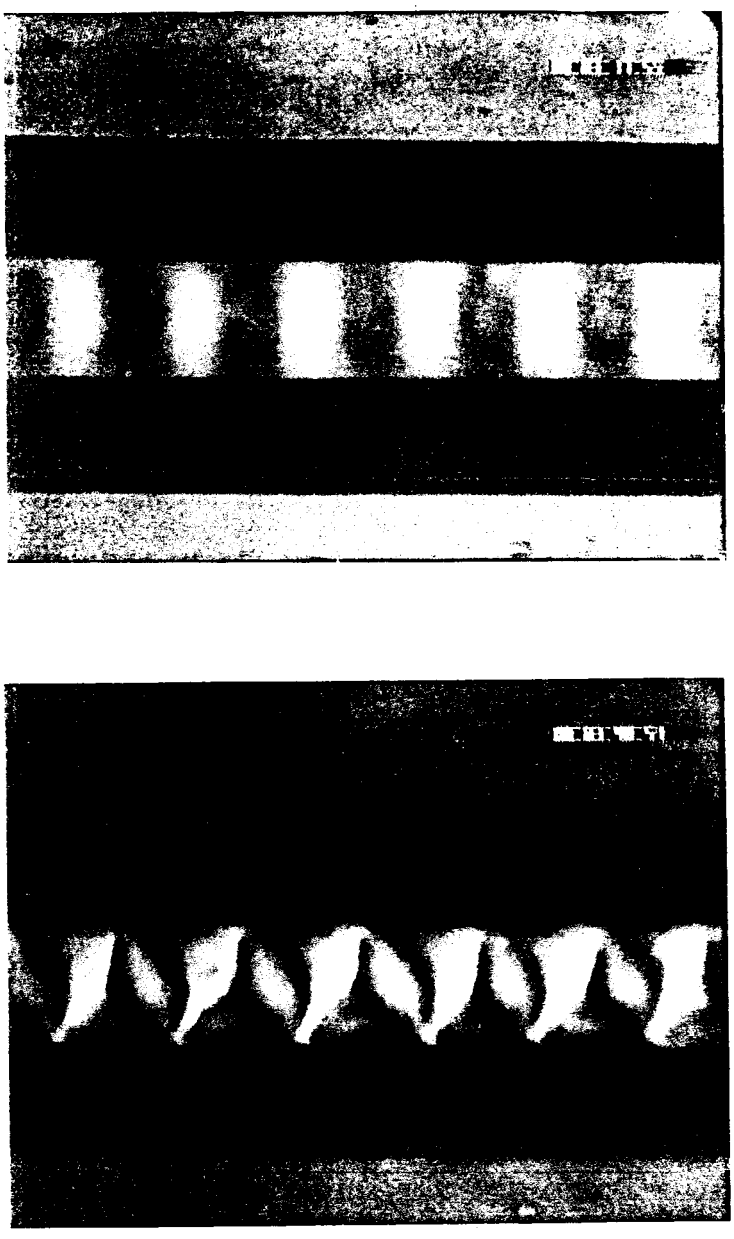

Fig.3.10: Videographs taken at 17 Hz with 10.0 volts with *(a)* polariser and analyser mutually crossed and (b) angle between polariser and analyser is 115 °. d=50 *pin* and interelectrode space = 65 μm.

Figures 3.11 and 3.12 show the threshold voltage (V_{th}) and reduced wave vector (q/p) in the conduction regime as functions of frequency of the applied field. The experimental trends agree with the theoretical ones (Figures 3.3 and 3.4). In figure 3.11 there is an initial decrease in the threshold voltage as the frequency of the applied field increases. This may possibly arise from a screening of the applied field at very low frequencies by impurity ions present in the sample. In the experimental curve we see a steep rise of V_{th} at frequencies above 800 Hz and hence for the purpose of comparing the experimental numbers with the theoretical ones, we estimate that the cut of frequency (f_c) is ≈1000 Hz. The calculated value of V_{th} at f/f_c=0.1 is 5.0 volt for a cell with an interelectrode space of 60 μm. This corresponds to an electric field of 830 V/cm. From the experimental curve (Fig. 3.11) obtained for a cell with an interelectrode space of 400 μm, V_{th} = 34 volt at the same reduced frequency. This is equivalent to an electric field of 850 V/cm which is quite close to the theoretical value. The ratio of V_{th} calculated at the reduced frequencies (f/f_c) of 0.1 and 0.8 is 0.5 from the theoretical curve (Fig.3.3) and is 0.57 from the experimental curve (Fig.3.9). Further the ratio of the wavevectors at f/f_c = 0.1 and 0.8 is 0.57 from the theroetical curve (Fig. 3.4) and it is 0.42 from experimental curve (Fig.3.12). Bearing in mind that all the calculations have been made using MBBA parameters, while the experiments have been conducted on a mixture for which many of the physical parameters are not known, the comparison between calculatetl and experimental data is quite adequate.

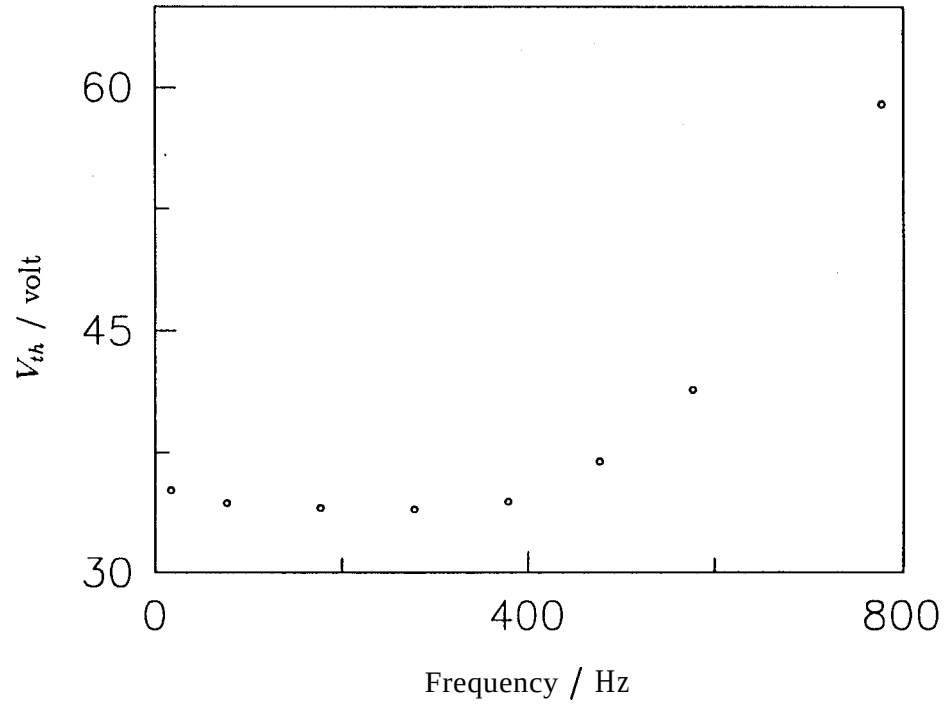

Fig.3.11: Experimentally observed variation of the threshold voltage (V_{th}) with frequency, for a cell of d=50 μm with interelectrode space = 406 μm at a temperature of **303** K.

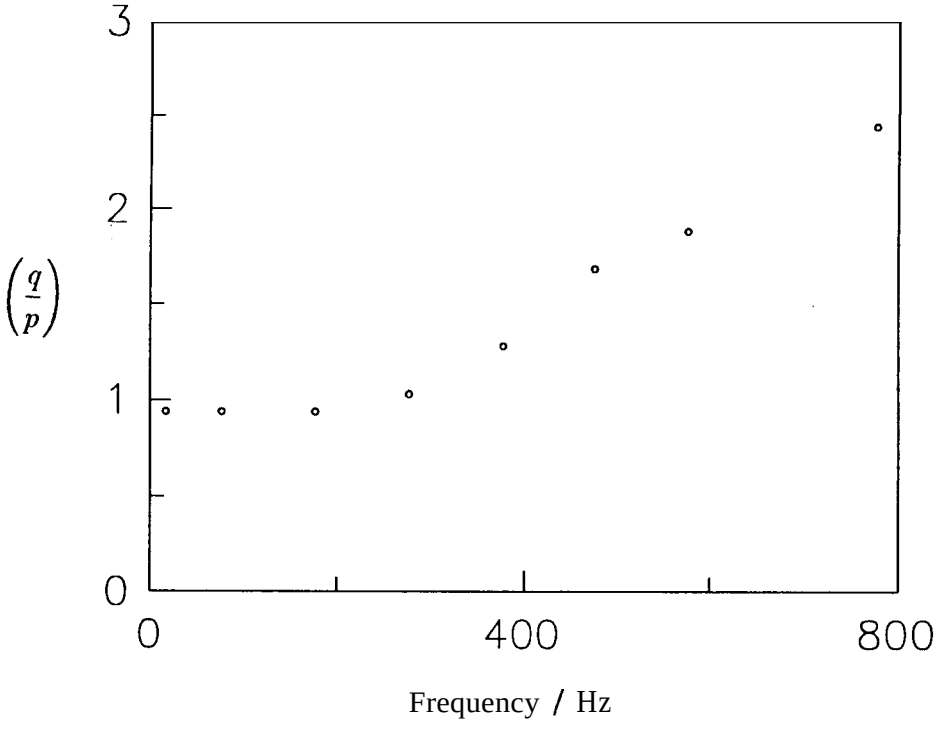

Fig.3.12: Experimentally observed variation of the reduced wavevector with frequency for the same cell as in Fig.3.11.

References

BLINOV,L.M., 1983, *Electro-optical and* Magneto-optical Properties of Liquid Crystals (Wiley).

BODENSCHATZ, E, ZIMMERMANN, W. and KRAMER,L., 1988, J. *Phys.* de Phys., 49, 1875.

CHISTYAKOV,I.G. and VISTIN, L.K., 1974, *Sov.Phys.Crystallogr.*, 19, 119.

DE GENNES,P.G., 1975, *The* Physics of Liquid Crystals (Clarendon).

DUBOIS-VIOLETTE,E., DE GENNES, P.G. and PARODI,O., 1971, J. de Phys., 32, 305.

DOZOV,I., MARTINOT-LAGARDE,Ph. and DURAND,G., 1982, *J. de Phys.*, 43, L365.

KRAMER,L., BODENSCHATZ,E., PESCH,W., THOM,W. and ZIMMERMANN, W., 1989, Liquid Crystals, 5, 699.

MADHUSUDANA,N.V. and DURAND,G., 1985, J. de Phys., 46, L195.

MADHUSUDANA,N.V., RAGHUNATHAN,V.A. and SUMATHY,K.R., 1987, Pramana - J. Phys., 28, L311.

MADHUSUDANA,N.V. and RAGHUNATHAN,V.A., 1988, Mol. *Cryst.* Liquid *Cryst.* Lett., 5, 201.

MAUGUIN,C., 1911, Bull. *Soc. Fr.* Miner. Crist., 34, 71.

PENZ, P.A. and FORD,G., 1972, Phys. Rev. *A,* 6, 414

SMITH,I.W., GALERNE,Y., LAGERWALL,S.T., DUBOIS-VIOLETTE,E. and DURAND,G., 1975, J. de Phys., 36, Cl-237

WILLIAMS,R., 1972, J. *Chem. Phys.*, 56, 147.